# Electronic Supplementary Information

## Experimental section

**Materials:** Chromium nitrate nonahydrate ($Cr(NO_3)_3 \cdot 9H_2O$), cobalt nitrate hexahydrate ($Co(NO_3)_2 \cdot 6H_2O$), urea, sodium chloride (NaCl), sodium carbonate ($Na_2CO_3$), ruthenium oxide ($RuO_2$), and nafion (5 wt.%) were bought from Aladdin Ltd. (Shanghai, China). Disodium phosphate anhydrous ($Na_2HPO_4$), potassium phosphate monobasic ($KH_2PO_4$), ethylenediaminetetraacetic acid disodium, potassium hydroxide (KOH), sodium hydroxide (NaOH), and N, N-diethyl-p-phenylenediamine (DPD) were obtained from Shanghai Maclin Biochemical Technology Co., Ltd. Acetone, ethanol, potassium permanganate ($KMnO_4$), sulfuric acid ($H_2SO_4$), and hydrochloric acid (HCl) were purchased from Beijing Chemical Reagent Co. Ltd (Beijing, China). Natural seawater was collected from Qingdao, Shandong, China, and most of the magnesium and calcium salts were removed by adding $Na_2CO_3$ in natural seawater before use. Ni foam (NF) was obtained from Shenzhen Green and Creative Environmental Science and Technology Co. Ltd. Ultrapure water was used throughout.

**Preparation of Cr-CoCH/NF:** Firstly, NF (2.0 × 3.0 $cm^2$) was sonicated in HCl, ethanol, and water for 10 min, respectively. The pretreated NF was put into a solution containing 2 mmol $Co(NO_3)_2 \cdot 6H_2O$, 10 mmol urea, and 35 mL water in a Teflon-lined autoclave and heated at 120 °C for 6 h to get CoCH/NF. The obtained CoCH/NF was then immersed in 0.01 M $Cr(NO_3)_3$ for 6 h. The above sample was finally taken out, washed with water, and dried at 60 °C for 2 h to obtain Cr-CoCH/NF.

**Preparation of $RuO_2$ on NF:** 5 mg $RuO_2$ was added in a solution containing 30 μL of nafion, 485 μL of ethanol, and 485 μL of water with the aid of ultrasonication (30 min) to form a homogeneous ink (5 mg $mL^{-1}$). 370 μL of catalyst ink was then dropped onto a piece of cleaned NF (0.5 × 0.5 $cm^2$) with a loading mass of 1.85 mg $cm^{-2}$.

**Characterizations:** XRD data were obtained via X-ray diffraction (XRD, Philip D8). Scanning electron microscopy (SEM, ZISS 300) equipped with an energy dispersive X-ray (EDX) facility, transmission electron microscopy (TEM, JEM-F200, JEOL Ltd.),

and X-ray photoelectron spectroscopy (XPS, ESCALAB 250 Xi) were utilized to research the morphology and compositions of samples. Inductive Coupled Plasma Emission Spectrometer (ICP-AES) (iCAD7400) were applied to study element content of sample. Absorbance data were acquired on UV-vis spectrophotometer (Shimadzu UV-2700).

**Electrochemical measurements:** Electrochemical OER tests were performed with a CHI 660E electrochemical workstation, using the prepared electrodes (0.5 × 0.5 $cm^2$), carbon rod, and Hg/HgO as the working electrode, counter electrode, and reference electrode, respectively. Three different electrolytes, including 1 M KOH, 1 M KOH + 0.5 M NaCl, and 1 M KOH + Seawater were used, and the pH was about 14.0. All measured potentials were referenced to that of reversible hydrogen electrode (RHE) ($E_{RHE} = E_{Hg/HgO} + 0.059 \times pH + 0.098$ V). The Tafel slope is calculated according to the Tafel equation as follows: $\eta = b \log j + a$, where η is overpotential, $j$ is the current density (mA $cm^{-2}$), and b is the Tafel slope (mV $dec^{-1}$). Electrochemical impedance spectroscopy measurements were performed between 100000 to 0.01 Hz with an amplitude of 5 mV. The catalytic activity of catalysts was determined by linear sweep voltammetry (LSV) curves with a scan rate of 2 mV $s^{-1}$. The double-layer capacitance ($C_{dl}$) values were obtained via cyclic voltammetry (CV) curves with the scan rates of 20−100 mV $s^{-1}$. All data (except for Figs. 3e, 4c, and S8) have been reported with 85% iR compensation.

**Determination of active chlorine**: The concentration of active chlorine in the electrolyte was determined based on DPD colorimetric method using a UV-vis spectrophotometer. DPD was added to the electrolyte solution after electrolysis at 500 mA $cm^{-2}$ for 12 h, and the electrolyte solution became pink. The absorbance at 550 nm was measured by UV-visible absorption spectroscopy, and the concentration of different active chlorine were also analyzed.

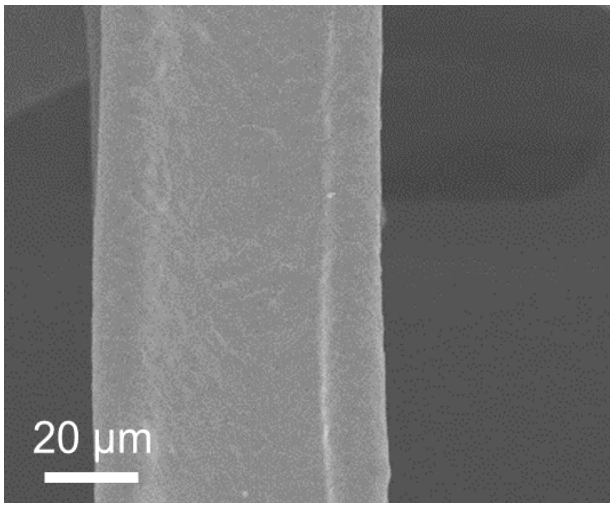


**Fig. S1.** SEM image of NF.

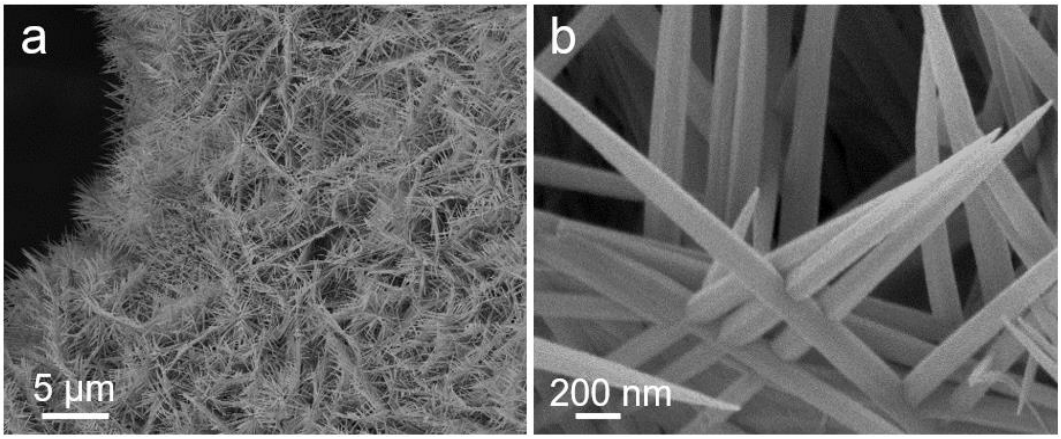


**Fig. S2.** (a) Low- and (b) high-magnification SEM images of CoCH/NF.

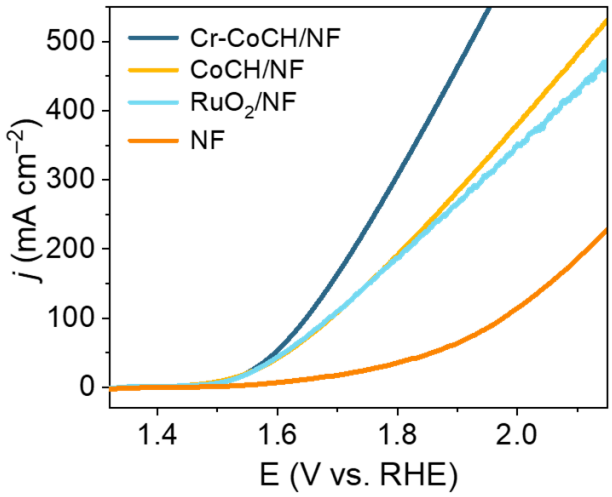


**Fig. S3.** LSV curves of different catalysts without iR compensation in 1 M KOH.

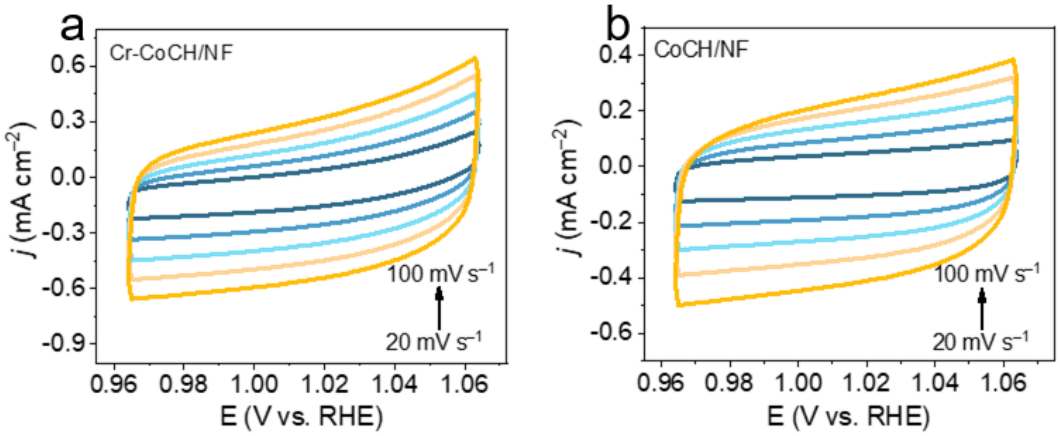


**Fig. S4.** CV curves of (a) Cr-CoCH/NF and (b) CoCH/NF in the double layer region at different scan rates of 20, 40, 60, 80 and 100 mV $s^{-1}$ in 1 M KOH.

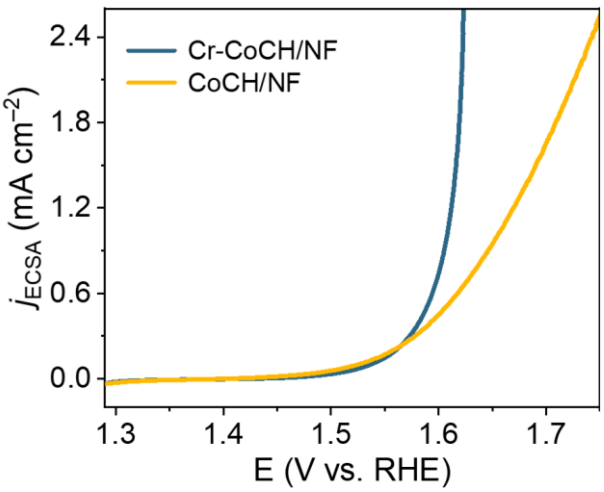


**Fig. S5.** LSV curves in 1 M KOH for Cr-CoCH/NF and CoCH/NF normalized by the electrochemical active surface area.

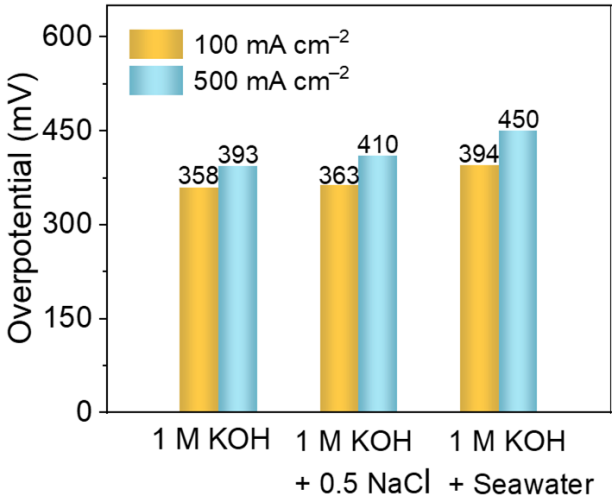


**Fig. S6.** The corresponding overpotentials of Cr-CoCH/NF tested in different electrolytes.

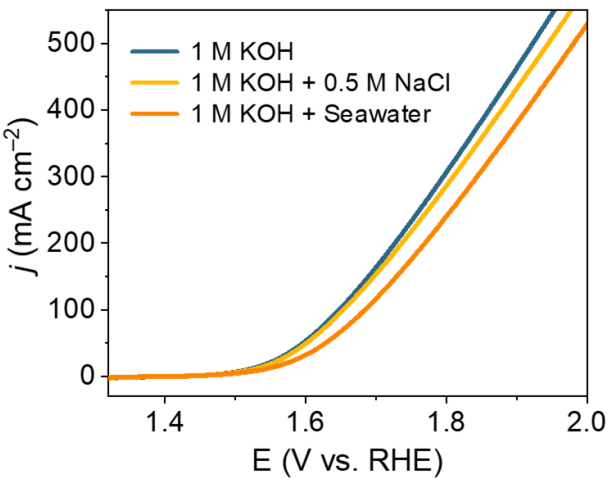


**Fig. S7.** LSV curves of Cr-CoCH/NF without iR compensation in different electrolytes.

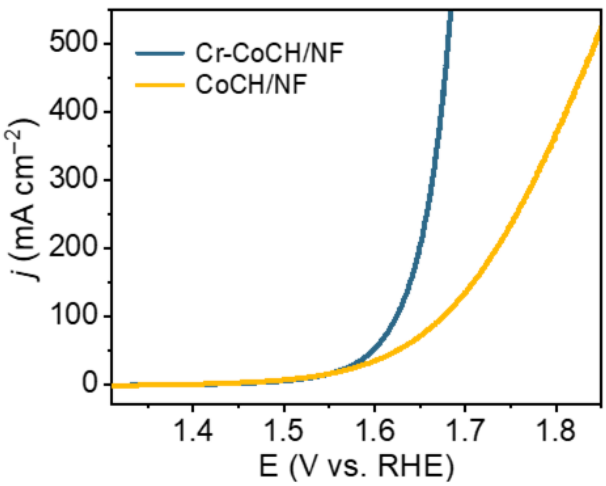


**Fig. S8.** LSV curves of Cr-CoCH/NF and CoCH/NF in 1 M KOH + Seawater.

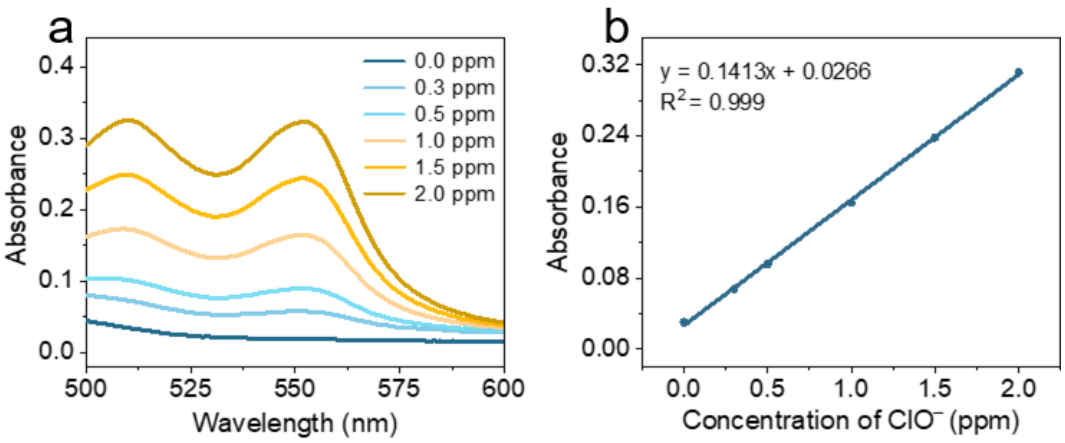


**Fig. S9.** (a) UV-vis absorption spectra of various active chlorine concentrations. (b) Calibration curve was used to evaluate $ClO^-$ concentrations of the electrolyte.

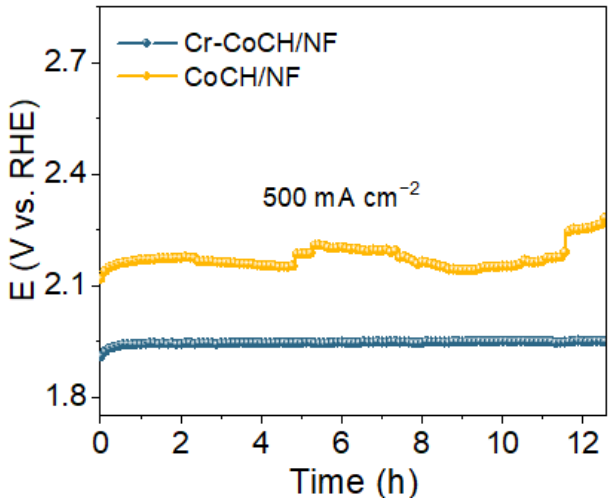


**Fig. S10.** Chronopotentiometry curves of Cr-CoCH/NF and CoCH/NF at a *j* of 500 mA cm$^{-2}$ without iR compensation in 1 M KOH + Seawater.

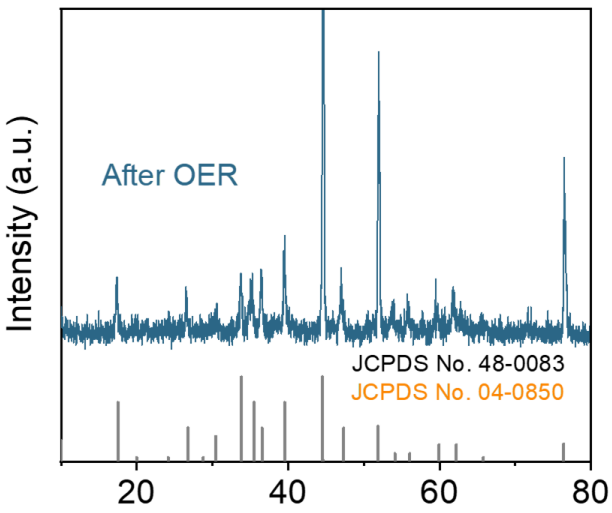


**Fig. S11.** XRD pattern of Cr-CoCH/NF after stability test in 1 M KOH + Seawater.

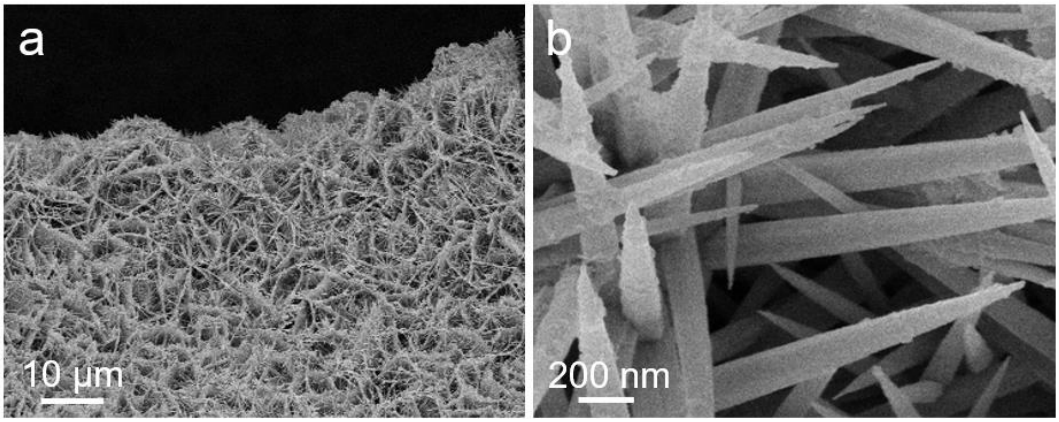


**Fig. S12.** (a) Low- and (b) high-magnification SEM images of Cr-CoCH/NF after stability test in 1 M KOH + Seawater.

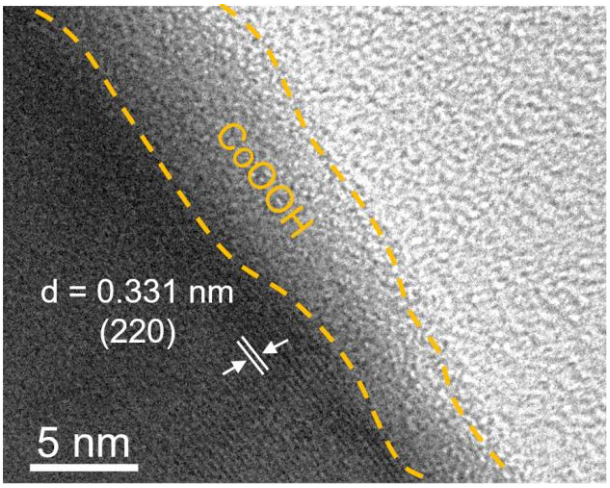


**Fig. S13.** HRTEM image of Cr-CoCH after stability test in 1 M KOH + Seawater.

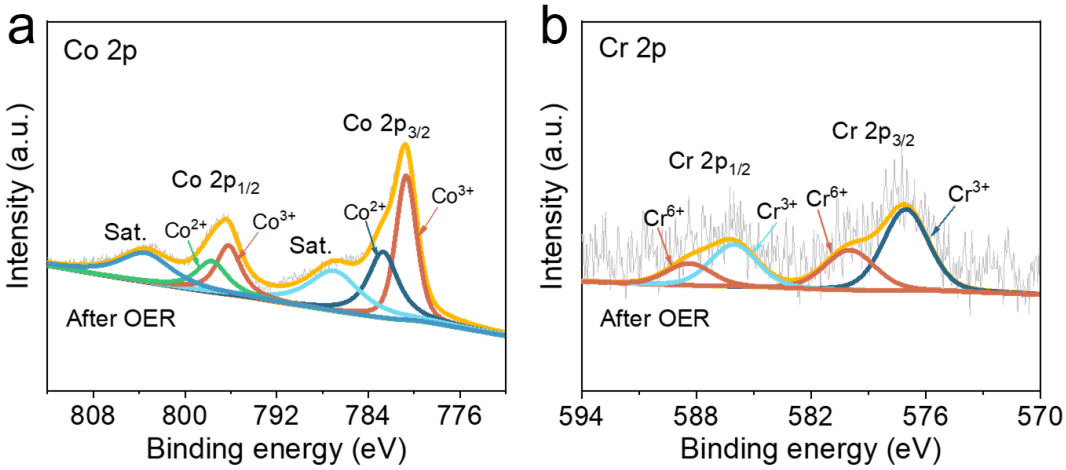


**Fig. S14.** High-resolution XPS spectra for Cr-CoCH in the (a) Co 2p and (b) Cr 2p regions after stability test in 1 M KOH + Seawater.

**Table S1.** Element analysis of Fe-CoCH/NF by ICP-AES.

| Element | Cr | Co |
|---|---|---|
| Element concentration (mg/L) | 5.29 | 0.71 |
| wt. (%) | 31.12 | 4.18 |

**Table S2.** Comparison of the OER performance of Cr-CoCH/NF with other reported seawater OER electrocatalysts.

| Catalysts | Electrolyte | Current Density (mA $cm^{-2}$) | Overpotential (mV) | Ref. |
|---|---|---|---|---|
| **Cr-CoCH/NF** | **1 M KOH + seawater** | **100**<br>**500** | **394**<br>**450** | **This work** |
| $Ag_2Se$-$Ag_2S$-CoCH/NF | 1 M KOH + seawater | 50<br>100 | 380<br>474 | 1 |
| Cr-$Co_xP$ | 1 M KOH + seawater | 100<br>500 | 334<br>392 | 2 |
| CoCrV LTHs | 1 M KOH + seawater | 100 | 395 | 3 |
| $Co_3O_4$<br>$Co_3S_4$ | 0.1 M KOH + 0.6 M NaCl | 10 | 503<br>366 | 4 |
| $Ni_3S_2$/$Co_3S_4$ | 1 M KOH + seawater | 100<br>500 | 360<br>440 | 5 |
| Co-Fe LDH | 1 M KOH + seawater | 10 | 530 | 6 |
| $Co_3O_4$-$Mn_2O_3$ | 1 M KOH + seawater | 10 | 500 | 7 |
| Fe-Co-S/$Cu_2O$/Cu | 1 M KOH + seawater | 100<br>200 | 440<br>520 | 8 |
| MoN-$Co_2N$ NSs | 1 M KOH + seawater | 100<br>500 | 357<br>432 | 9 |
| NiCoHPi@$Ni_3N$/NF | 1 M KOH + seawater | 100<br>500 | 396<br>474 | 10 |
| Co-N,P-HCS | 1 M KOH + seawater | 100 | 490 | 11 |
| $CoSe_2$-NCF | 1 M KOH + seawater | 10<br>100 | 245<br>455 | 12 |
| $CoP_x$@FeOOH | 1 M KOH + seawater | 100<br>500 | 283<br>337 | 13 |
| Co-Fe-O-B | 1 M KOH + 0.5 M NaCl | 100 | 434 | 14 |
| $Ni(OH)_2$-TCNQ/GP | 1 M KOH + seawater | 100<br>500 | 382<br>542 | 15 |

## References


1 L. Yang, C. Feng, C. Guan, L. Zhu and D. Xia, *Appl. Surf. Sci.*, 2023, **607**, 154885.

2 Y. Song, M. Sun, S. Zhang, X. Zhang, P. Yi, J. Liu, B. Huang, M. Huang and L. Zhang, *Adv. Funct. Mater.*, 2023, 2214081.

3 S. Khatun and P. Roy, *Chem. Commun.*, 2022, **58**, 1104–1107.

4 J. Li, F. Xu, K. Wang, J. He, Y. Wang, L. Lei, M. Zhu, L. Zhuang and Z. Xu, *Chem. Eng. Sci.*, 2023, **267**, 118366.

5 C. Wang, M. Zhu, Z. Cao, P. Zhu, Y. Cao, X. Xu, C. Xu and Z. Yin, *Appl. Catal. B-Environ.*, 2021, **291**, 120071.

6 F. Cheng, X. Feng, X. Chen, W. Lin, J. Rong and W. Yang, *Electrochim. Acta*, 2017, **251**, 336–343.

7 L. Bigiani, D. Barreca, A. Gasparotto, T. Andreu, J. Verbeeck, C. Sada, E. Modin, O. I. Lebedev, J. R. Morante and C. Maccato, *Appl. Catal. B-Environ.*, 2021, **284**, 119684.

8 J. Sun, P. Song, H. Zhou, L. Lang, X. Shen, Y. Liu, X. Cheng, X. Fu and G. Zhu, *Appl. Surf. Sci.*, 2021, **567**, 150757.

9 X. Wang, X. Han, R. Du, C. Xing, X. Qi, Z. Liang, P. Guardia, J. Arbiol, A. Cabot and J. Li, *ACS Appl. Mater. Interfaces*, 2022, **14**, 41924–41933.

10 H. Sun, J. Sun, Y. Song, Y. Zhang, Y. Qiu, M. Sun, X. Tian, C. Li, Z. Lv and L. Zhang, *ACS Appl. Mater. Interfaces*, 2022, **14**, 22061–22070.

11 X. Wang, X. Zhou, C. Li, H. Yao, C. Zhang, J. Zhou, R. Xu, L. Chu, H. Wang, M. Gu, H. Jiang and M. Huang, *Adv. Mater.*, 2022, **34**, 2204021.

12 H. Chen, S. Zhang, Q. Liu, P. Yu, J. Luo, G. Hu and X. Liu, *Inorg. Chem. Commun.*, 2022, **146**, 110170.

13 L. Wu, L. Yu, B. McElhenny, X. Xing, D. Luo, F. Zhang, J. Bao, S. Chen and Z. Ren, *Appl. Catal. B-Environ.*, 2021, **294**, 120256.

14 S. Gupta, M. Forster, A. Yadav, A. J. Cowan, N. Patel and M. Patel, *ACS Appl. Energy Mater.*, 2020, **3**, 7619–7628.

15 L. Zhang, J. Wang, P. Liu, J. Liang, Y. Luo, G. Cui, B. Tang, Q. Liu, X. Yan, H. Hao, M. Liu, R. Gao and X. Sun, *Nano Res.*, 2022, **15**, 6084–6090.